Nanoscale

PAPER

View Article Online
View Journal | View Issue

Cite this: *Nanoscale*, 2016, **8**, 11275

Compact quantum dot–antibody conjugates for FRET immunoassays with subnanomolar detection limits†

Lucia Mattera,‡[a,b,c] Shashi Bhuckory,‡[d] K. David Wegner,§[d] Xue Qiu,[d] Fabio Agnese,[a,e] Christophe Lincheneau,[a,b,c] Tim Senden,[a,b,c] David Djurado,[a,b,c] Loïc J. Charbonnière,[f] Niko Hildebrandt*[d] and Peter Reiss*[a,b,c]

A novel two-step approach for quantum dot (QD) functionalization and bioconjugation is presented, which yields ultra-compact, stable, and highly luminescent antibody–QD conjugates suitable for use in FRET immunoassays. Hydrophobic InPZnS/ZnSe/ZnS (emission wavelength: 530 nm), CdSe/ZnS (605 nm), and CdSeTe/ZnS (705 nm) QDs were surface functionalized with zwitterionic penicillamine, enabling aqueous phase transfer under conservation of the photoluminescence properties. Post-functionalization with a heterobifunctional crosslinker, containing a lipoic acid group and a maleimide function, enabled the subsequent coupling to sulfhydryl groups of proteins. This was demonstrated by QD conjugation with fragmented antibodies (F(ab)). The obtained F(ab)–QD conjugates range among the smallest antibody-functionalized nanoprobes ever reported, with a hydrodynamic diameter <13 nm, PL quantum yield up to 66% at 705 nm, and colloidal stability of several months in various buffers. They were applied as FRET acceptors in homogeneous, time-gated immunoassays using Tb-antibodies as FRET donors, both coupled by an immunological sandwich complex between the two antibodies and a PSA (prostate specific antigen) biomarker. The advantages of the compact surface coating for FRET could be demonstrated by an 6.2 and 2.5 fold improvement of the limit of detection (LOD) for PSA compared to commercially available hydrophilic QDs emitting at 605 and 705 nm, respectively. While the commercial QDs contain identical inorganic cores responsible for their fluorescence, they are coated with a comparably thick amphiphilic polymer layer leading to much larger hydrodynamic diameters (>26 nm without biomolecules). The LODs of 0.8 and 3.7 ng mL^{-1} obtained in 50 μL serum samples are below the clinical cut-off level of PSA (4 ng mL^{-1}) and demonstrate their direct applicability in clinical diagnostics.

Received 21st April 2016,
Accepted 27th April 2016

DOI: 10.1039/c6nr03261c

www.rsc.org/nanoscale

Introduction

Colloidal quantum dots (QDs) are widely used as fluorescent labels for biosensing. They possess unique optical properties, which make them interesting alternatives to traditionally used organic dyes or fluorescent proteins. Among the most outstanding properties are their size-dependent, narrow photoluminescence (PL) bands, high PL quantum yields, spectrally broad and strong absorption (resulting in a large effective Stokes shift), and their long-term resistance against photobleaching.[1,2] These assets have made QDs one of the most versatile fluorophores for multiplexed and sensitive biosensing,[3–5] and in particular for Förster resonance energy transfer (FRET)-based biosensing.[5–11] Within the huge variety of QD-FRET biosensing applications for the analysis of biomolecular interactions, homogeneous sandwich immunoassays, which quantify biomarkers *via* two different antibodies (ABs) that engage in FRET upon biomarker recognition, range among the most selective and sensitive but also the most

[a]*Univ. Grenoble Alpes, INAC-SyMMES, F-38054 Grenoble Cedex 9, France*
[b]*CEA, INAC-SyMMES, Laboratoire STEP, 17 rue des Martyrs, F-38054 Grenoble Cedex 9, France. E-mail: peter.reiss@cea.fr*
[c]*CNRS, SPrAM, F-38054 Grenoble Cedex 9, France*
[d]*NanoBioPhotonics (nanofret.com), Institut d'Electronique Fondamentale, Université Paris-Sud, Université Paris-Saclay, CNRS, 91405 Orsay Cedex, France. E-mail: niko.hildebrandt@u-psud.fr*
[e]*CEA, INAC-MEM, LEMMA, 17 rue des Martyrs, F-38054 Grenoble Cedex 9, France*
[f]*Institut Pluridisciplinaire Hubert Curien (IPHC), UMR 7178 CNRS/UdS, Laboratoire d'Ingénierie Moléculaire Appliquée à l'Analyse (LIMAA), ECPM, 25, rue Becquerel, 67087 Strasbourg Cedex 2, France*

†Electronic supplementary information (ESI) available: SI-1: UV-vis/PL spectra; SI-2: TEM images; SI-3: DLS; SI-4: gel electrophoresis; SI-5: FTIR spectra; SI-6: overlap between QD absorption spectra and area-normalized Tb emission; SI-7: photographs of the samples; and optical characterization of QD–F(ab) conjugates (Table S1). See DOI: 10.1039/c6nr03261c

‡These authors contributed equally.

§Present address: CEA, INAC-SyMMES, 17 rue des Martyrs, F-38054 Grenoble Cedex 9, France.

challenging systems. This is because the relatively large sizes of ABs (*ca.* 10 nm in length) and QDs (depending on their emission wavelength and surface coatings) plus the connection of the ABs *via* a biomarker (often proteins with sizes of up to several nm) lead to long distances between the QDs and their FRET partners. FRET immunoassays have been developed with QD-donors[12–19] as well as QD-acceptors.[11,20–24] The latter case is of particular interest, because these FRET assays used Tb-complexes as donors, whose extremely long excited-state lifetimes allow for time-gated detection and a concomitant suppression of directly excited QD PL and autofluorescence background.[3,8,9] Such Tb-to-QD energy transfer systems have been shown to follow FRET theory[25,26] and were successfully used in various homogeneous FRET biosensing applications, ranging from molecular rulers,[27,28] over nucleic acid detection and enzyme kinetics,[29,30] to molecular logic gates.[31] Tb-to-QD FRET immunoassays could already provide multiplexing capability and clinically relevant limits of detection (LODs) in serum samples.[11,20] However, beyond these proof-of-concept studies, the major limitations for developing QD-FRET immunoassays with LODs competitive to commercial kits are: (i) insufficient colloidal stability of compact QDs in biological media, (ii) thick QD surface coatings (*e.g.*, PEG, polymer, or lipid coatings that protect the inorganic QD from the biological environment and render them hydrosoluble), and (iii) insufficient AB-conjugation strategies for QDs with thinner organic capping. The latter two QD surface related aspects result in long FRET donor–acceptor distances and unfavorable binding conditions, respectively. This leads to lower sensitivities compared to conventional time-resolved (TR)-FRET immunoassays that use lanthanide donor and dye acceptor AB conjugates.[32] The development of QD–AB conjugates with compact surface functionalization for aqueous phase transfer and high-performance photophysical properties for efficient FRET immunoassays in serum samples would therefore present a milestone of the utmost importance for the integration of QDs into clinical *in vitro* diagnostics.

Here, we present a novel QD functionalization and bioconjugation approach, which yields stable and highly luminescent QD–antibody conjugates for improved TR-FRET immunoassays. Aqueous phase transfer of lab-synthesized InPZnS/ZnSe/ZnS QDs emitting at 530 nm and commercial CdSe/ZnS and CdSeTe/ZnS QDs (Life Technologies) emitting at 605 and 705 nm was achieved by surface ligand exchange with penicillamine (Pen). These wavelengths have been selected as they result in minimal interference with the emission of the Tb-complexes used as the FRET donor. Under optimized conditions, ligand exchange with Pen results in a very compact (~1 nm) organic surface layer while preserving high PL quantum yields. The zwitterionic Pen also provides low non-specific binding with serum proteins and very high colloidal stability of several years in aqueous buffers. For sulfhydryl-reactive QD–AB conjugation, we further functionalized the QD surface with a bifunctional ligand (Mal1) containing a lipoic acid anchoring function and a maleimide group, spaced by three poly(ethylene) glycol (PEG) moieties. The bidentate (reduced) lipoic acid function is able to substitute Pen molecules and provides excellent stability of the Mal1 ligand on the QD surface. Successful conjugation of the prepared QDs with fragmented antibodies F(ab), further reducing the size of the sandwich immunocomplexes, was characterized by optical spectroscopy, dynamic light scattering (DLS), agarose gel electrophoresis, and FTIR. To demonstrate the advantages of the ultra-compact (hydrodynamic diameter <13 nm), stable, and strongly fluorescent QD–AB conjugates for clinical diagnostics, we performed Tb-to-QD FRET immunoassays for the detection of prostate specific antigen (PSA) in 50 μL serum samples on a commercially available clinical fluorescence plate reader (KRYPTOR). The achieved LODs down to 0.8 ng mL^{-1} are 2.5 fold lower than the best Tb-to-QD PSA FRET immunoassays reported so far, which were performed under identical conditions but with the commercially available ITK-Qdots (Life Technologies). The latter differ from our QDs only by their surface coating: a comparably thick organic layer composed of amphiphilic polymers, which yields QDs with hydrodynamic radii of more than 26 nm (without conjugated biomolecules).[28] Our results are the first demonstration of using compact surface-ligand capped QDs for homogeneous FRET immunoassays that can outperform the commercial QD "gold standard" and function under clinically relevant conditions (50 μL serum samples measured on a clinical plate reader). Comparing the 0.8 ng mL^{-1} LOD with the clinical cut-off level of PSA (4 ng mL^{-1})[33] clearly shows the immediate applicability of the compact QD nanoprobes for PSA diagnostics.

Experimental section

Chemicals

D-Penicillamine, tetramethylammonium hydroxide (TMAOH), phosphate-buffered saline solution (10× PBS), 0.5 M tris(2-carboxyethyl)phosphine hydrochloride solution (TCEP), tris(hydroxymethyl)aminomethane (TRIS/Cl), bovine serum albumin (BSA), agarose powder, indium acetate (99.99%), myristic acid (>99%), tris(trimethylsilyl)phosphine (95%), 1-dodecanethiol (97%), and 1-octadecene (90%) were purchased from Sigma-Aldrich. Zinc stearate (90%) was acquired from Riedel de Haën. MAL-dPEG3-lipoic acid (Mal1) was purchased from Quanta Biodesign. QD CdSe 605 and 705 were purchased from Life Technologies/Thermo Fisher[34] while the NHS-activated terbium complex (Lumi4-Tb) was provided by Lumiphore in lyophilized form. Prostate specific antigen (PSA) and monoclonal primary antibodies against PSA (IgGs: "PSR222" and "PSS233") were provided by Cezanne/Thermo Fisher. Solvents were purchased from Aldrich, Fluka, and Acros, and used without further purification. All water solutions were prepared from ultrapure laboratory grade water (resistivity 18 MΩ cm) that was filtered and purified using a Millipore MilliQ cartridge system and autoclaved.

Instruments

Absorption and emission spectra were recorded on the following spectrometers: HP 8452A and Perkin Elmer Lambda 35 for UV-Vis absorption; Hitachi F-4500 fluorescence spectrophoto-

meter equipped with a 150 W xenon lamp and an excitation monochromator as well as a PicoQuant Fluotime 300 for photoluminescence (PL). Decay curves were acquired on the Fluotime 300 and fitted using EasyTau (PicoQuant). The hydrodynamic diameter (by dynamic light scattering) and zeta potential of the NCs dispersed in water were measured using a Malvern Zetasizer (NanoZS). Fourier transform infrared (FTIR) spectra were taken on a Perkin Elmer Paragon 500 spectrometer equipped with an attenuated total reflection (ATR) setup. Gel images were acquired using a Gel Doc XR system (Bio-Rad, Hercules, CA). HRTEM analyses were performed on a JEOL 3010 working at 300 kV, equipped with a LaB_6 gun and a Gatan Orius SC 200 2k × 2k CCD camera.

InPZnS/ZnSe/ZnS QD synthesis

The synthesis of InPZnS/ZnSe/ZnS alloy core gradient shell nanocrystals is based on reported procedures.[35,36] All procedures except for nanocrystal purification have been carried out under an inert atmosphere.

Preparation of precursor solutions. For the preparation of the indium myristate ($In(MA)_3$) stock solution (0.1 M), 1 mmol of anhydrous indium acetate was mixed with 3 mmol of myristic acid (MA) and 10 mL of 1-octadecene (ODE) in a 50 mL three-neck flask equipped with a condenser. The mixture was heated to 100–120 °C for 1 h under vacuum until an optically clear solution was obtained. After backfilling the flask with Ar and cooling to room temperature, the turbid solution of indium myristate was stored in a glovebox. For the zinc oleate ($Zn(OA)_2$) stock solution (0.4 M), 5 mmol of zinc acetate, 10 mmol of oleic acid (OA) and 9.35 mL of ODE were loaded into a 50 mL three-neck flask and the same procedure as for the preparation of $In(MA)_3$ was followed. The zinc stearate ($Zn(St)_2$) stock solution (0.1 M) was prepared by heating 1 mmol of $Zn(St)_2$ with 10 mL of ODE at 120 °C for 1 h. A 0.4 M TOPSe stock solution was prepared by the dissolution of 2 mmol Se powder in 5 mL of trioctylphosphine (TOP) under stirring for 24 h. A TOPS stock solution was prepared with the same procedure using elemental sulfur.

Synthesis of InPZnS alloy nanocrystals. In a glovebox, 1 mL of the $In(MA)_3$ stock solution (0.1 mmol $In(MA)_3$), 1 mL of the $Zn(St)_2$ stock solution (0.1 mmol), 0.1 mmol of 1-dodecanethiol (DDT) and 7.5 mL of ODE were added to a 50 mL three-neck flask. Afterwards the flask was equipped with a condenser and connected to a Schlenk line. Next, the mixture was heated under vigorous stirring to 300 °C with a ramp of around 60 °C min^{-1} using a molten salt bath. When the temperature inside the flask reached 100 °C, 0.1 mmol of tris(trimethylsilyl) phosphine ($P(TMS)_3$), diluted with 1 mL of ODE, were injected. During the heating, NC formation is visible by the color change of the reaction mixture to dark yellow/orange. After 30 min, the reaction mixture was cooled to below 220 °C to stop growth.

Growth of a ZnSe/ZnS gradient shell. For the ZnSe/ZnS gradient shell growth, a 10 fold excess of precursors was used with respect to the core synthesis, and a Se : S ratio of 0.2. Briefly, $Zn(OA)_2$ (1 mmol, 2.5 mL of the 0.4 M stock solution) was added dropwise to the reactive mixture at 220 °C. This was followed by the successive injection of TOP-Se (0.2 mmol, 0.5 mL of the 0.4 M solution) and TOP-S (0.8 mmol, 2 mL of the 0.4 M solution). The resulting mixture was heated to 300 °C within 10 minutes and then kept at this temperature for 20 min. After cooling down to room temperature, purification of the QDs was performed *via* three cycles of precipitation/redispersion. First, 10 mL of a 1 : 1 (v/v) mixture of chloroform/methanol and 100 mL of acetone was added. Then the resulting suspension was centrifuged (8000 rpm for 5 minutes), the supernatant discarded and the obtained solid dispersed in 5 mL of chloroform. Finally, the QDs can be dispersed and stored in a variety of organic solvents, like hexane, toluene or chloroform.

Purification before phase transfer. Thorough purification of the initial QDs, enabling the complete removal of excess surface ligands or side-products is crucial for successful phase transfer. 1 mL of the InPZnS/ZnSe/ZnS QDs in chloroform was mixed with anhydrous ethanol (1 mL) and centrifuged at 10 000 rpm for 2 minutes. The clear solution of supernatant was discarded and the precipitate was dispersed in 1 mL of chloroform. This cycle was repeated three times. For the commercial CdSe/ZnS-based QDs in decane the solvent was changed to chloroform prior to phase transfer. 4 mL of a methanol/isopropanol (3 : 1 v : v) mixture were added to 1 mL of the QD colloidal solution and centrifuged for 2 min at 10 000 rpm. The supernatant was discarded and the resulting pellet dispersed in 1 mL of chloroform.

Phase transfer. A 0.2 M solution of penicillamine (containing 200 μL of 0.5 M TCEP) was prepared in 1 mL of degassed MilliQ water (18 MΩ cm). The pH was adjusted to 9 by dropwise addition of 0.5 M TMAOH. 500 μL of the phase transfer solution was mixed with 1 mL of a 3–5 μM colloidal solution of QDs in chloroform. The biphasic mixture was stirred vigorously at ~1400 rpm for 2 h at room temperature. At the end of the transfer, affording QD–Pen, the biphasic mixture results either in a clear separation of two phases or in an emulsion. In the latter case, the mixture is centrifuged at 5200 rpm for 1 min to obtain a clear phase separation. The QDs in the (upper) aqueous phase are separated from the (lower) organic phase.

Purification and storage. A NAP™-5-10,-25 size exclusion column (Sephadex™ G-25 DNA Grade from GE Healthcare) was vertically clamped and equilibrated according to the manufacturer's protocol. QDs in water were added and after being adsorbed on the gel bed, they were eluted using 1× PBS buffer and kept at 4 °C in the dark for storage.

Post-functionalization. Solutions of Mal1 (1 mL, 10 mM) and TCEP (0.046 mL, 0.5 M) in degassed water were added to a suspension of QD–Pen (0.5 mL, 5.2 μM in degassed water) and the pH was adjusted to 7.0 by dropwise addition of 0.5 M TMAOH. The mixture was vortexed at 800 rpm overnight at room temperature. The resulting fine suspension was purified by size exclusion chromatography with NAP™-10,-25 columns (Sephadex™ G-25 DNA Grade from GE Healthcare). The obtained QD-Mal1 were then concentrated under vacuum or by using a 30 kDa molecular weight cut-off (MWCO) spin column from Millipore, centrifuging at 4000*g* for 4 min with a final volume of 400 μL. Storage at 4 °C as above.

Preparation of QD–F(ab) conjugates

IgGs were fragmented to F(ab) using a Pierce™ Mouse IgG F(ab′) $F(ab')_2$ preparation kit following the instructions provided by the supplier. Prior to conjugation of the QDs to the F(ab)s in a molar ratio of 1 : 20, disulfide bonds of the latter were reduced to sulfhydryls with 5 mM of TCEP in 1× PBS by mixing for 30 minutes at 30 rpm at room temperature. Purification from excess TCEP was performed using Zeba 7K spin columns (Thermo Fisher) according to the manufacturer's protocol. The resulting purified F(ab) was then mixed with the QDs in 1× PBS and incubated for 4 hours while rotating at 30 rpm at RT. Conjugates were washed from unbound F(ab)s 4 times with 1 mL 1× PBS pH 7.5 using a 100 kDa MWCO spin column from Millipore at 1000*g*. Supernatants were taken after a final centrifugation at 4000*g* for 5 minutes.

QD PL quantum yields

The absolute fluorescence QYs of the QDs were determined by comparison with a standard of known QY (freshly prepared solution of Fluorescein 548 in 0.1 M NaOH; QY = 93%, Rhodamine 6G in ethanol; QY = 95%[37] or QD705 in chloroform; QY = 92%[34]). The QY was calculated with the following formula:

$$\Phi_{NC} = \Phi_{Standard}(a_{NC}/a_{Standard})(n_{NC}{}^2/n_{Standard}{}^2)$$

where Φ is the QY, a the gradient (slope) of the plot of the integrated fluorescence intensity *vs.* absorbance and n the refractive index of the solvent (1.375 for hexane, 1.446 for chloroform, 1.333 for water and buffer and 1.36 for ethanol[37]). All spectra were corrected for the instrumental response with calibration curves furnished by the supplier and the estimated errors on QY are ±15% of the calculated values. Aliquots or purified samples of the QDs in hexane, chloroform or water were put into 1 cm quartz cuvettes and diluted until the absorbance at the excitation wavelength was around 0.1. At least four samples of different concentrations were prepared and measured for determining the slopes. Both the sample and the reference were excited at 460 nm for InP based QDs and at 480 nm for CdSe based QDs.

Hydrodynamic size and dispersibility of QDs

The hydrodynamic diameter of the water-soluble QDs was measured by dynamic light scattering (Malvern Zetasizer NanoZS). Multiple runs (>3) were performed and averaged, and the QDs in 1× PBS buffer were filtered (0.22 μm) prior to the measurements. The spectra have been corrected by the instrument software for viscosity (0.882 mPa s at 25 °C), absorption (0.01), solvent (water) refractive index (1.33) and material refractive index (assumed as 2.7 and 2.45 for In- and Cd-based QDs, respectively[38]). The data were collected in automatic mode and expressed in number %. The zeta potential was measured using the same instrument under zeta potential settings.

Gel electrophoresis

A 1% gel was prepared in 25 mM Hepes buffer (pH 7.4) and poured in a 10.7 × 5.2 cm gel tray levelled in a gel caster (RunOne System). A comb (12 wells) was placed into the gel. The gel was allowed to cool down to room temperature and to solidify within at least 1 hour. The comb was removed and the gel was taken out of the casting device and placed into the electrophoresis device which was filled with 25 mM Hepes buffer pH 7.4 until the whole gel was covered. The samples were mixed with about 20% of their volume with the loading buffer (30% glycerol in 25 mM Hepes buffer with 0.3% Orange G) and carefully filled into the wells. The electrophoresis devices were run at a constant voltage of 100 V. After 5, 10, 15 and 30 min an image was taken placing the gel on a UV transilluminator (Gel Doc XR system, Bio-Rad).

FRET immunoassays

All FRET assays contained 50 μL of each AB–Tb and QD–AB conjugate (in 10 mM TRIS/HCl; 0.5% BSA pH 7.4) at constant concentrations, to which 50 μL of serum with increasing concentrations of TPSA was added. The homogeneous FRET immunoassays were measured on a modified "KRYPTOR compact plus" clinical fluorescence plate reader from Cezanne/Thermo Fisher. The reader simultaneously detects the time-gated PL intensities, in a time window from 100 μs to 900 μs, in the Tb donor and the QD acceptor channels.

Results and discussion

Surface functionalization of the QDs

Initially the strongly fluorescent InP-based or CdSe-based QDs were capped with hydrophobic organic surfactants rendering them soluble in non-polar media. Aqueous phase transfer is a critical step to make these QDs usable in biological studies. Two factors are of prime importance with regard to the phase transfer protocol: first, the procedure needs to guarantee a minimum loss of fluorescence quantum yield; second, it should provide high colloidal stability preventing the aggregation of QDs. Many literature protocols and commercial products rely on the encapsulation of the QDs with bulky amphiphilic polymers, which leads to hydrodynamic diameters in the range of 15–20 nm or more. Here, we focus on direct ligand exchange, which yields a much more compact surface coating beneficial for FRET applications. In the first step, the QDs were transferred from the organic to the aqueous phase by means of penicillamine (Pen), following a procedure we reported earlier.[39] It relies on the use of a biphasic mixture of QDs in chloroform and Pen in an aqueous solution of precisely controlled pH in the presence of the mild reducing agent TCEP. Basic pH is required for achieving the deprotonation of the Pen thiol group, which results in stronger binding to the surface of the different ZnS-coated QDs, while TCEP prevents Pen disulfide formation. Quantitative phase transfer was visible by the mutual color change of both phases (*cf.* Fig. 1a). In a second step, post-functionalization with the bifunctional ligand Mal1 was carried out under reduction of the disulfide group by means of TCEP (Fig. 1b).[40] The bidentate lipoic acid group provides stronger binding to the QD

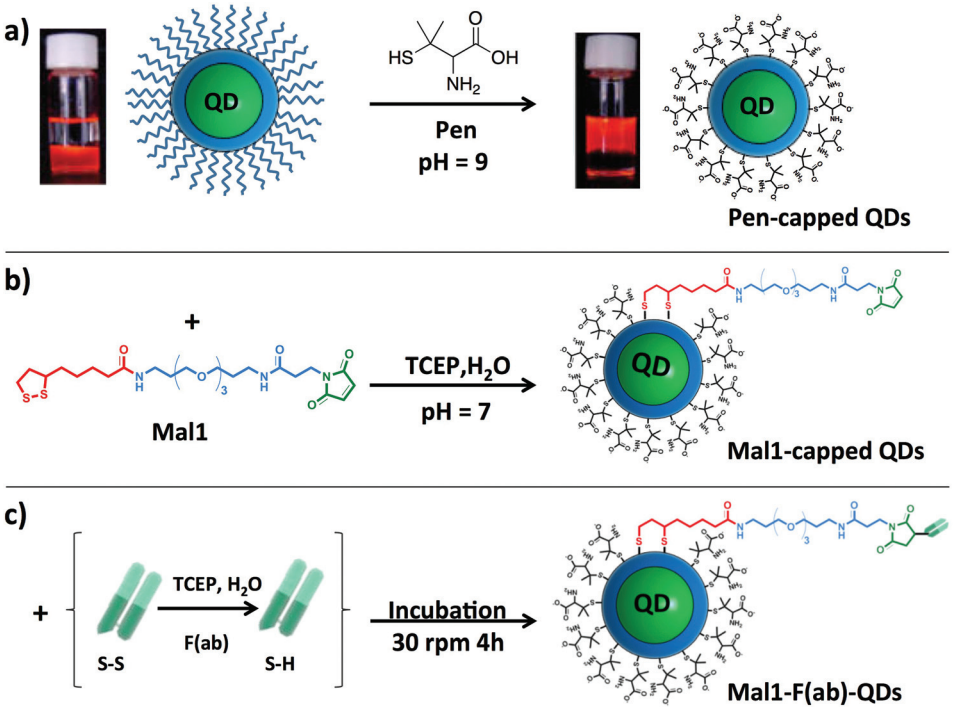

Fig. 1 Schematic representation of (a) the aqueous phase transfer of QDs with penicillamine (Pen), (b) post-functionalization with Mal1, and (c) subsequent conjugation to sulfhydryl groups of fragmented antibodies (F(ab)).

surface than Pen molecules, facilitating introduction of Mal1.[41] The short polyethyleneglycol chain improves hydrosolubility and adds a spacer, which makes the maleimide functions stick out of the Pen corona and hence easily available for subsequent antibody conjugation. The full structural and photophysical characterization of the Pen- and Mal1-functionalized QDs is included in the next section.

QD–antibody conjugates

NHS-functionalized Tb complexes (Lumi4-Tb) were directly labeled to available primary amines of anti-PSA IgG ABs (Tb–AB), whereas the coupling of the smaller (*ca.* 50 kDa) fragmented F(ab) to the QDs employed sulfhydryl chemistry, which was previously shown to result in functional QD–AB conjugates for biosensing[11,20,42,43] and is known to be highly efficient and provide stable linkage.[40,44] The reactive maleimide functionalities introduced onto the QD surface target free biomolecular thiols, such as those obtained by fragmentation of IgG to F(ab). This approach allows for the formation of QD–AB conjugates that retain the QD optical properties and the specific and selective AB-antigen recognition capability.[45] F(ab)s were first activated through reduction of the S–S bond by TCEP and the maleimide group of Mal1 was then coupled with the free thiol group of the reduced F(ab) to form a covalent thio-ether bond (Fig. 1c).[40] The same functionalization and post-functionalization approach was implemented for the linkage of F(ab) to all types of QDs studied, namely InPZnS/ZnSe/ZnS, CdSe/ZnS, and CdSeTe/ZnS. A Tb per IgG conjugation ratio of 11 ± 3 was determined by UV-Vis absorption spectroscopy using the molar absorptivities of Lumi4-Tb (ε(340 nm) = 26 000 M^{-1} cm^{-1}) and IgGs (ε(280 nm) = 210 000 M^{-1} cm^{-1}) and Beer–Lambert's law (Fig. 2a). The comparison of Tb–AB with the unconjugated complex shows no alteration of the PL properties after AB-conjugation. Upon excitation at 365 nm the PL spectrum of Tb–AB shows the characteristic Tb emission lines and the obtained decay curve had an almost single exponential decay with an average PL lifetime of *ca.* 2.6 ms (Fig. 2a).

Surface functionalization of the QDs with Pen and post-functionalization with Mal1 did not lead to significant modifications of the UV-vis and PL spectra (Fig. SI-1†). On the other hand, a decrease of the PL QY was observed, from 0.40 (QD530), 0.60 (QD605), and 0.92 (QD705) in chloroform to 0.27, 0.30, and 0.66, respectively. The absorption and PL spectra of the three QD–AB conjugates are shown in Fig. 2b–d. QD concentrations were determined using the molar absorptivities of $\varepsilon_{450\ nm}$(QD530) = 4.2 × 10^5 M^{-1} cm^{-1} (experimentally determined), $\varepsilon_{405\ nm}$(QD605) = 2.8 × 10^6 M^{-1} cm^{-1} and $\varepsilon_{405\ nm}$(QD705) = 8.3 × 10^6 M^{-1} cm^{-1} (provided by the supplier).[34] The photophysical properties of the QDs were slightly altered by the F(ab) conjugation, as summarized in Table S1,† compared to the Pen-capped QDs. A PL red shift of 4 nm could be detected for the CdSe-based QD605 and QD705, while a blue shift of 3 nm was found for the InP-based QD530. Further experiments are needed to unequivocally elucidate the origin of these shifts; we tentatively ascribe them to the quantum confined Stark effect, induced by the change of the dielectric environment of the QDs upon conjugation with F(ab).[46] AB-conjugation also led to changes in the PL lifetimes (Table S1†)

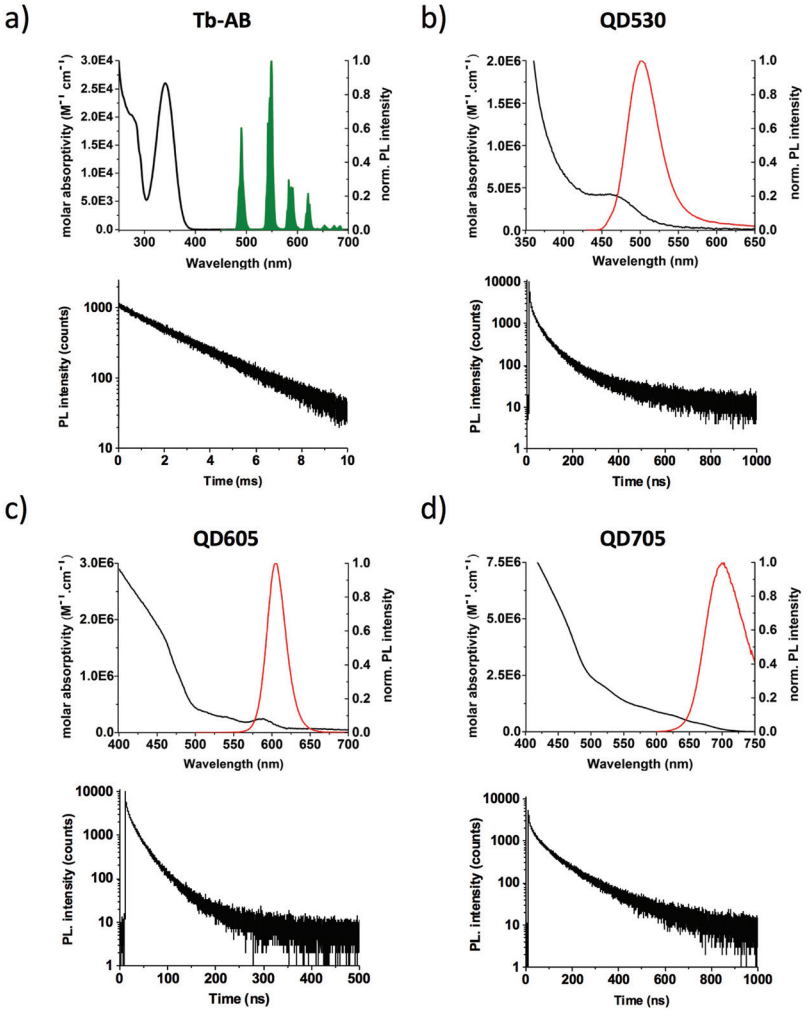

Fig. 2 (a) Top: absorption (black line) and PL (green, excitation wavelength 365 nm) spectra of Tb–AB conjugate. Bottom: Tb–AB PL decay curve (490 ± 0.5 nm) upon pulsed excitation at 365 nm with a repetition rate of 100 Hz. Amplitude-averaged decay time: τ(Tb) = 2.6 ± 0.3 ms. (b–d) Top: absorption (black) and PL (red) spectra; bottom: PL decay curves of F(ab)-conjugated InPZnS/ZnSe/ZnS (QD530), CdSe/ZnS (QD605), and CdSeTe/ZnS (QD705) QDs in 1× PBS buffer. Amplitude-averaged PL lifetimes: τ(QD530) = 17.7 ± 2.8 ns, τ(QD605) = 10.4 ± 1.1 ns, and τ(QD705) = 40.7 ± 6.4 ns.

from 24 to 18 ns for QD530, from 4.6 to 10 ns for QD605, and from 79 to 41 ns for QD705. These changes are attributed to the generation or filling of electronic trap states acting as competing deexcitation channels upon F(ab) attachment.

Sizes and morphologies of the inorganic parts of the QDs were characterized using transmission electron microscopy (TEM), which revealed nearly monodisperse spherical (QD530 and QD605) and elongated (QD705) nanocrystals (Fig. SI-2†). The hydrodynamic diameters of the QDs were evaluated by dynamic light scattering (DLS). As exemplified by QD705 (*cf.* Fig. SI-4†), these measurements confirmed the narrow size distribution observed with TEM and revealed small hydrodynamic diameters, which slightly increase with each functionalization step. Introduction of the Mal1 ligand led to a size increase from 8 to 10 nm with respect to QD705-Pen, which was in the expected range for a ligand with an approximate length of 3.0 nm. Conjugation with F(ab) led to a further increase to 13 nm as the total hydrodynamic diameter, which makes this QD–AB conjugate one of the smallest AB-functionalized near-infrared (NIR) emitting nanoprobes ever reported. Colloidal stability of the QDs in water or relevant buffer solutions is of crucial importance for biological detection. The obtained Pen- and Mal1-functionalized QDs showed no sign of aggregation after storage of more than two years at 4 °C in the dark in 1× PBS buffer (pH = 7.4), as confirmed by combined periodical DLS and UV-Vis measurements. After F(ab) conjugation the colloidal stability was determined to be at least 2 months, which is the current limit of our measurements. The photophysical and morphological characterization results show that our approach of using an optimized ligand exchange with Pen, followed by post-functionalization with Mal1, is an efficient and simple way of obtaining highly luminescent, stable, and compact QDs ready for further functionalization with small F(ab)s to yield very small fluorescent AB-nanoprobes. Gel electrophoresis (Fig. SI-4†) and FTIR (Fig. SI-5†) measurements further confirmed successful post-functionalization with Mal1

and F(ab) conjugation of the QDs. For all QDs, the bands on the agarose gel corresponding to the QD–F(ab) conjugates were the most retarded due to the larger sizes of the QD–AB conjugates. FTIR clearly revealed, by comparison to the free, *i.e.* not QD-bound, molecules, peaks corresponding to the carbonyl stretch vibrations of the maleimide function in QD-Mal1 and to the N–H stretch vibration of F(ab) in QD-Mal1-F(ab). In these characterizations all three types of QDs behaved in the same way, which was expected as they mainly differ in the inorganic core composition but all possess an identical ZnS outer shell and the same first ligand exchange procedure with Pen has been used.

FRET immunoassays

To demonstrate the functionality of the compact QD–AB conjugates, we performed homogeneous Tb-to-QD FRET immunoassays against PSA on the KRYPTOR compact plus clinical fluorescence plate reader (Cezanne/Thermo Fisher). PL intensities of Tb (I_{Tb}) and QDs (I_{QD}) were acquired simultaneously in a time-gated detection window between 100 μs to 900 μs after pulsed excitation at 337 nm using a nitrogen laser operating at 20 Hz. Due to the extremely long PL lifetimes of Tb (ms) compared to QDs (ns), the time-gating allows efficient suppression of short-lived sample autofluorescence and direct excitation of the QDs. This allows for solely obtaining the pure FRET signals (FRET-quenched Tb PL and FRET-sensitized QD PL). Optical bandpass filters (Delta and Semrock) for the Tb donor and QD acceptor detection channels were (494 ± 10) nm for Tb and (522 ± 6) nm, (607 ± 4) nm, and (707 ± 8) nm for QD530, QD605 and QD705, respectively. The FRET-ratio was defined as:

$$\text{FRET-ratio} = \frac{I_{QD}(100\text{–}900\ \mu s)}{I_{Tb}(100\text{–}900\ \mu s)}$$

Within all the FRET-assays the Tb–AB and QD–AB concentrations were kept constant (3 nM Tb–AB with 3 nM QD605–AB or QD705–AB, and 9 nM Tb–AB with 9 nM QD530–AB) while PSA concentrations, prepared in serum, ranged from 0.05 nM (for QD605 and QD705) or 0.1 nM (for QD530) to 9 nM. 50 μL of each AB-conjugate (Tb–AB and QD–AB) were mixed with 50 μL of serum for a total working volume of 150 μL. The three immunoassay calibration curves (FRET-ratio over total PSA concentration) are presented in Fig. 3. All three assays showed a steep FRET-ratio increase with increasing PSA concentration up to *ca.* 2 to 4 nM, which was expected due to the saturation of Tb–QD FRET complexes (in the concentration range of Tb–AB or QD–AB). It should be noted that the FRET-ratio increase was very small (only *ca.* 5% at the maximum) for the Tb–QD530 assay, which was most probably related to the lower Förster distance of Tb–QD530 (R_0 = 6.1 nm) compared to the values of Tb–QD605 (R_0 = 7.7 nm) and Tb–QD705 (R_0 = 11 nm). These findings can be understood by analyzing the overlap integrals of the different D–A pairs (Fig. SI-6†). Therefore, only the latter two FRET systems (for which the FRET-ratio increases were *ca.* 45% and 100% at maximum) could be used for a quantitative evaluation of PSA immunoassays (Fig. 3b and c).

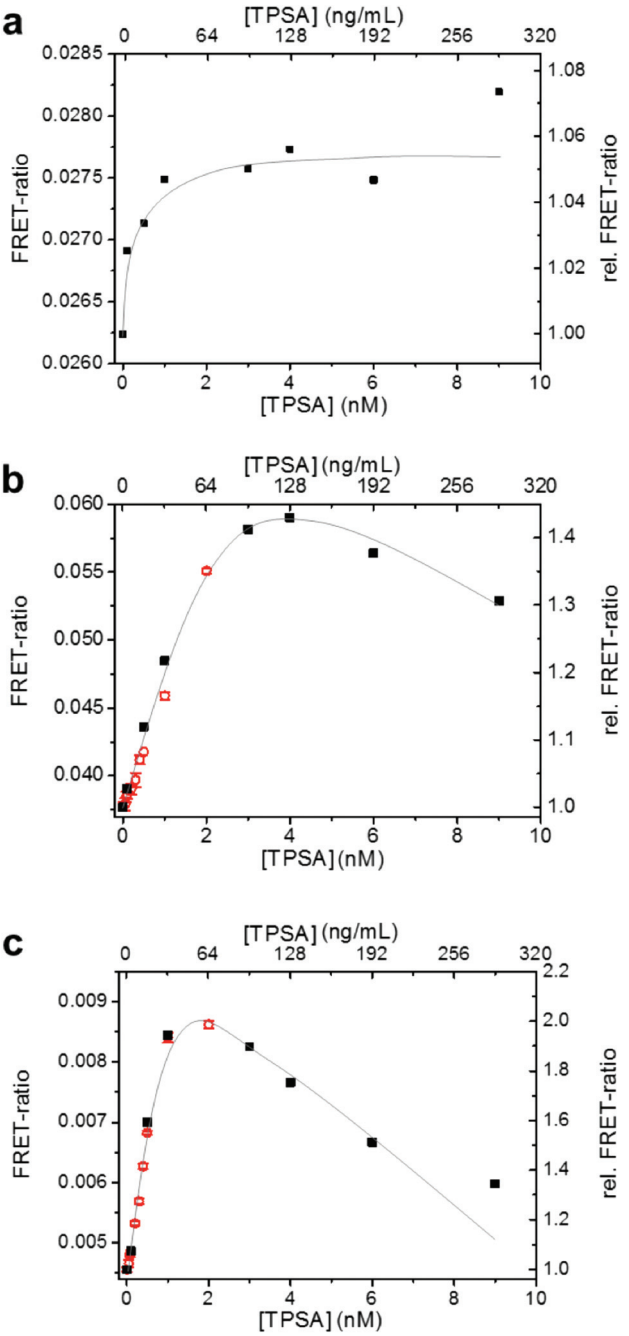

Fig. 3 Calibration curves for total PSA (TPSA) homogeneous FRET immunoassays using the Tb–QD530 (a), Tb–QD605 (b), and Tb–QD705 (c) FRET pairs. The assays in (b) and (c) could be used for quantitative analysis. Black data points (squares) were from a first set of experiments using PSA concentrations between 0 and 9 nM. Red data points (circles) were taken in a second set of experiments for a statistical analysis of LODs in the linearly increasing parts of the assay curves. Grey lines in the graphs are trend lines meant as a guide to the eye.

A first assay calibration curve over a concentration range of 0 to 9 nM (black squares) revealed a linear FRET-ratio increase, followed by saturation and a FRET-ratio decrease. This decrease is due to the so-called Hook-effect, describing the increase of the fraction of single fluorophore (Tb–AB–PSA and

Table 1 Förster distances R_0 and LODs of Tb–QD FRET immunoassays against PSA

Donor-AB	Acceptor-AB	R_0 (nm)	LOD (nM)	LOD (ng mL^{-1}) compact QDs (this study)	LOD[a] (ng mL^{-1}) Qdot ITK™ amino PEG	Clinical cut-off level of PSA
Tb-IgG	QD605-F(ab)	7.7	0.12	3.7	23	4 ng mL^{-1}
Tb-IgG	QD705-F(ab)	11.0	0.02	0.8	2.0	

[a] Taken from ref. 20. Same Tb–QD FRET immunoassays against PSA, which used the same commercial QDs but with a thick PEG/polymer coating (as provided by the supplier).

QD–AB–PSA) binding complexes compared to FRET (Tb–AB–PSA–QD–AB) binding complexes. Homogeneous FRET assays are usually designed for the detection of very low concentrations without any washing or separation steps. To access the very low concentration range, high signal-to-background ratios are required and therefore the Tb–AB concentrations are selected in a low nM range (in our case 3 nM) to keep the Tb PL background at a minimum intensity level. As a consequence, the dynamic detection range becomes relatively narrow (*ca.* 0.05 to 2 nM in our case). On the KRYPTOR clinical plate reader used in our study, this drawback is overcome by a kinetic sample detection and automated dilution of too highly concentrated samples,[11] which can increase the dynamic detection range by several orders of magnitude. A second calibration curve, with many more PSA concentrations in the linearly increasing parts of the assay curves (red circles), was used to determine the LODs (three times the standard deviation of the FRET-ratio from PSA-free samples divided by the slope of the linearly increasing part of the calibration curve in the 0 to 1 nM concentration range). All samples for the statistical analysis were prepared and measured in triplicate (n = 9) apart from the PSA-free samples which were prepared 10 times and measured in triplicate (n = 30). Table 1 summarizes the Förster distances and LODs obtained for the Tb–QD605 and Tb–QD705 FRET pairs, as well as LOD values obtained for the same Tb-to-QD FRET immunoassays against PSA using the readily surface-coated (thick PEG/polymer coating) hydrophilic QD605 and QD705 from the same supplier (Life Technologies). Both Tb–QD assays with compact QDs provide LODs below the clinical cut-off value for PSA (4 ng mL^{-1}),[33] and these LODs are also 6.2 and 2.5 fold lower compared to the same assays using the larger commercial QDs. It should be noted that the FRET assays, performed on a clinical plate reader, use ratiometric time-gated PL detection, which is known to provide very low coefficients of variation.[47] The 6.2 and 2.5 fold improvements are therefore very significant, particularly when taking into account the very low and clinically relevant concentrations, and the results confirm the superior performance of our compact QD–AB conjugates for homogeneous FRET immunoassays using serum samples.

Conclusions

In this study we presented a two-step procedure for the preparation of compact, highly luminescent, and colloidally stable QDs that were further used for the simple and functional conjugation with fragmented ABs (F(ab)), to yield one of the smallest fluorescent AB–nanoparticle conjugates to be used for FRET reported to date. In the first step, aqueous phase transfer was achieved by ligand exchange with the zwitterionic penicillamine. The second post-functionalization step introduced a bifunctional ligand, which contained reactive maleimide functions. The latter could be used for the selective and stable conjugation to sulfhydryl groups on ABs. Although this bioconjugation strategy was demonstrated only with InPZnS/ZnSe/ZnS, CdSe/ZnS, and CdSeTe/ZnS core/shell QDs and F(ab) antibodies, it is applicable to any kind of nanoparticle containing surface atoms with binding affinity for thiolate ligands and biomolecules containing sulfhydryl groups (*e.g.*, on available cysteines). The immediate applicability of the compact QD–AB conjugates to biosensing was demonstrated in homogeneous FRET immunoassays against PSA, using Tb–ABs as FRET donors and the QD–ABs as FRET acceptors, both coupled by an immunological sandwich complex between the two ABs and the PSA biomarker. Detection of PSA in 50 μL serum samples with subnanomolar (20 pM = 0.8 ng mL^{-1}) detection limits showed the clinically relevant concentration range, over which these FRET immunoassays can be applied. Not only were the LODs of two Tb–QD FRET immunoassays (using 605 nm and 705 nm emitting QDs) well below the clinical cut-off value of PSA (4 ng mL^{-1}), the utilization of the compact QD–AB conjugates also provided a 6.2 and 2.5 fold sensitivity improvement compared to the same commercially available QDs that were purchased with a standard PEG/polymer-based coating. These highly sensitive and homogeneous Tb-to-QD FRET immunoassays are suitable for any other biomarker against which two specific ABs exist. Our results show that the compact QD–AB conjugates have a large potential for improving diagnostic applications, and given the multiplexing capability of Tb–QD FRET,[7,29] we are confident that these small nanoparticle–AB fluorescent probes will become important players in clinical *in vitro* diagnostics.

Acknowledgements

The authors thank Emilie Rustique for assistance with DLS and zeta-potential measurements, Lumiphore, Inc. for Lumi4®-Tb-NHS reagents, Cezanne/Thermo Fisher for immunoassay reagents, PSA, and anti-PSA antibodies, the

Chinese Scholarship Council for funding the PhD fellowship of X.Q., and the Agence Nationale de la Recherche (Grant number ANR-12-NANO-0007 NanoFRET) for financial support.

References

1 Y. Yin and A. P. Alivisatos, *Nature*, 2005, **437**, 664–670.
2 A. P. Alivisatos, *Science*, 1996, **271**, 933–937.
3 N. Hildebrandt, K. D. Wegner and W. R. Algar, *Coord. Chem. Rev.*, 2014, **273–274**, 125–138.
4 W. R. Algar, H. Kim, I. L. Medintz and N. Hildebrandt, *Coord. Chem. Rev.*, 2014, **263–264**, 65–85.
5 K. D. Wegner and N. Hildebrandt, *Chem. Soc. Rev.*, 2015, **44**, 4792–4834.
6 W. R. Algar, D. Wegner, A. L. Huston, J. B. Blanco-Canosa, M. H. Stewart, A. Armstrong, P. E. Dawson, N. Hildebrandt and I. L. Medintz, *J. Am. Chem. Soc.*, 2012, **134**, 1876–1891.
7 D. Geißler, L. J. Charbonnière, R. F. Ziessel, N. G. Butlin, H. G. Löhmannsröben and N. Hildebrandt, *Angew. Chem., Int. Ed.*, 2010, **49**, 1396–1401.
8 L. J. Charbonnière and N. Hildebrandt, *Eur. J. Inorg. Chem.*, 2008, **2008**, 3241–3251.
9 D. Geißler, S. Linden, K. Liermann, K. D. Wegner, L. J. Charbonnière and N. Hildebrandt, *Inorg. Chem.*, 2014, **53**, 1824–1838.
10 D. Geißler, S. Stufler, H. G. Löhmannsröben and N. Hildebrandt, *J. Am. Chem. Soc.*, 2013, **135**, 1102–1109.
11 K. D. Wegner, Z. Jin, S. Linden, T. L. Jennings and N. Hildebrandt, *ACS Nano*, 2013, **7**, 7411–7419.
12 F. A. Esteve-Turrillas and A. Abad-Fuentes, *Biosens. Bioelectron.*, 2013, **41**, 12–29.
13 S. Ge, L. Ge, M. Yan, X. Song, J. Yu and S. Liu, *Biosens. Bioelectron.*, 2013, **43**, 425–431.
14 M. D. Kattke, E. J. Gao, K. E. Sapsford, L. D. Stephenson and A. Kumar, *Sensors*, 2011, **11**, 6396–6410.
15 F. Long, C. Gu, A. Z. Gu and H. Shi, *Anal. Chem.*, 2012, **84**, 3646–3653.
16 J. Qian, C. Wang, X. Pan and S. Liu, *Anal. Chim. Acta*, 2013, **763**, 43–49.
17 Q. Wei, M. Lee, E. K. Lee, X. Yu, G. H. Seong, J. Choo and Y. W. Cho, *Anal. Biochem.*, 2006, **358**, 31–37.
18 C. Zhang, D. Gao, G. Zhou, L. Chen, X.-A. Zhang, Z. Cui and Z. He, *Chem. – Asian J.*, 2012, **7**, 1764–1767.
19 H. Zhang, Q. Zeng, X. Liu, X. Kong, Y. Zhang and L. Tu, *Chem. Commun.*, 2012, **48**, 1781–1783.
20 S. Bhuckory, O. Lefebvre, X. Qiu, K. D. Wegner and N. Hildebrandt, *Sensors*, 2016, **16**, 197.
21 M.-J. Chen, Y.-S. Wu, G.-F. Lin, J.-Y. Hou, M. Li and T.-C. Liu, *Anal. Chim. Acta*, 2012, **741**, 100–105.
22 Z.-H. Chen, Y.-S. Wu, M.-J. Chen, J.-Y. Hou, Z.-Q. Ren, D. Sun and T.-C. Liu, *J. Fluoresc.*, 2013, **23**, 8449–8457.
23 H. Härmä, T. Soukka, A. Shavel, N. Gaponik and H. Weller, *Anal. Chim. Acta*, 2007, **604**, 177–183.
24 K. D. Wegner, S. Lindén, Z. Jin, T. L. Jennings, R. E. Khoulati, P. M. P. van Bergen en Henegouwen and N. Hildebrandt, *Small*, 2014, **10**, 734–740.
25 N. Hildebrandt, L. J. Charbonnière, M. Beck, R. F. Ziessel and H.-G. Löhmannsröben, *Angew. Chem., Int. Ed.*, 2005, **44**, 7612–7615.
26 L. J. Charbonnière, N. Hildebrandt, R. F. Ziessel and H.-G. Löhmannsröben, *J. Am. Chem. Soc.*, 2006, **128**, 12800–12809.
27 F. Morgner, D. Geißler, S. Stufler, N. G. Butlin, H.-G. Löhmannsröben and N. Hildebrandt, *Angew. Chem., Int. Ed.*, 2010, **49**, 7570–7574.
28 K. D. Wegner, F. Morgner, E. Oh, R. Goswami, K. Susumu, M. H. Stewart, I. L. Medintz and N. Hildebrandt, *Chem. Mater.*, 2014, **26**, 4299–4312.
29 X. Qiu and N. Hildebrandt, *ACS Nano*, 2015, **9**, 8449.
30 W. R. Algar, A. P. Malanoski, K. Susumu, M. H. Stewart, N. Hildebrandt and I. L. Medintz, *Anal. Chem.*, 2012, **84**, 10136–10146.
31 J. C. Claussen, N. Hildebrandt, K. Susumu, M. G. Ancona and I. L. Medintz, *ACS Appl. Mater. Interfaces*, 2014, **6**, 3771–3778.
32 H. Bazin, M. Préaudat, E. Trinquet and G. Mathis, *Spectrochim. Acta, Part A*, 2001, **57**, 2197–2211.
33 K. L. Greene, P. C. Albertsen, R. J. Babaian, H. B. Carter, P. H. Gann, M. Han, D. A. Kuban, A. O. Sartor, J. L. Stanford, A. Zietman and P. Carroll, *J. Urol.*, 2013, **189**, S2–S11.
34 *The Molecular Probes Handbook, A Guide to Fluorescent Probes and Labeling Technologies*, Thermo Fisher Scientific, 11th edn, 2010.
35 L. Li and P. Reiss, *J. Am. Chem. Soc.*, 2008, **130**, 11588–11589.
36 J. Lim, W. K. Bae, D. Lee, M. K. Nam, J. Jung, C. Lee, K. Char and S. Lee, *Chem. Mater.*, 2011, **23**, 4459–4463.
37 R. Sjoback, J. Nygren and M. Kubista, *Spectrochim. Acta, Part A*, 1995, **51**, L7–L21.
38 M. J. Weber, *Handbook of optical materials*, CRC Press, Boca Raton, 2003.
39 S. Tamang, G. Beaune, I. Texier and P. Reiss, *ACS Nano*, 2011, **5**, 9392–9402.
40 G. Hermanson, *Bioconjugate Techniques*, Academic Press, 1996.
41 K. Susumu, H. T. Uyeda, I. L. Medintz, T. Pons, J. B. Delehanty and H. Mattoussi, *J. Am. Chem. Soc.*, 2007, **129**, 13987–13996.
42 T. L. Jennings, S. G. Becker-Catania, R. C. Triulzi, G. Tao, B. Scott, K. E. Sapsford, S. Spindel, E. Oh, V. Jain, J. B. Delehanty, D. E. Prasuhn, K. Boeneman, W. R. Algar and I. L. Medintz, *ACS Nano*, 2011, **5**, 5579–5593.
43 T. L. Jennings, R. C. Triulzi, G. Tao, Z. E. St Louis and S. G. Becker-Catania, *Sensors*, 2011, **11**, 10557–10570.
44 D. H. Marrian, *J. Chem. Soc.*, 1949, 1515–1516.
45 M. Arruebo, M. Valladares and Á. González-Fernández, *J. Nanomater.*, 2009, **2009**, 1–24.
46 U. T. D. Thuy, N. Q. Liem, D. X. Thanh, M. Protière and P. Reiss, *Appl. Phys. Lett.*, 2007, **91**, 241908.
47 G. Mathis, *Clin. Chem.*, 1993, **39**, 1953–1959.